Studying the (α,p)-process in X-Ray Bursts using Radioactive Ion Beams

Catherine M. Deibel

Joint Institute for Nuclear Astrophysics
Michigan State University

Physics Division
Argonne National Laboratory

Type I X-Ray Bursts (XRBs)

Neutron stars:
1.4 M_o, 10 km radius

Normal star

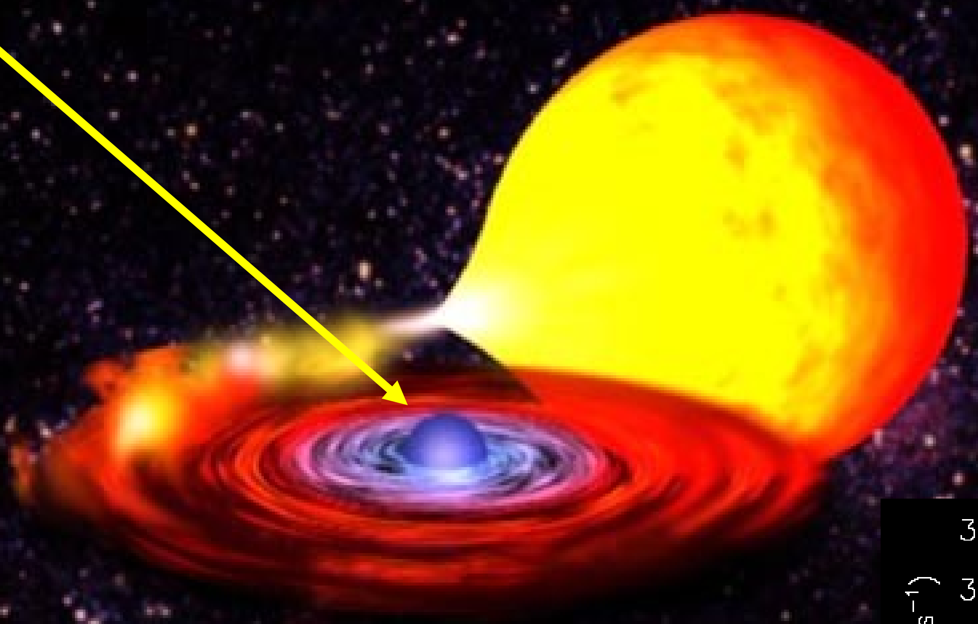

Accretion rate ~ $10^{-8}/10^{-10}$ M_o/year

Peak x-ray burst temperature ~ 1.5 GK

Recurrence rate ~ hours to days

Burst duration of 10 – 100 s

Observed x-ray outburst ~10^{39} – 10^{49} ergs

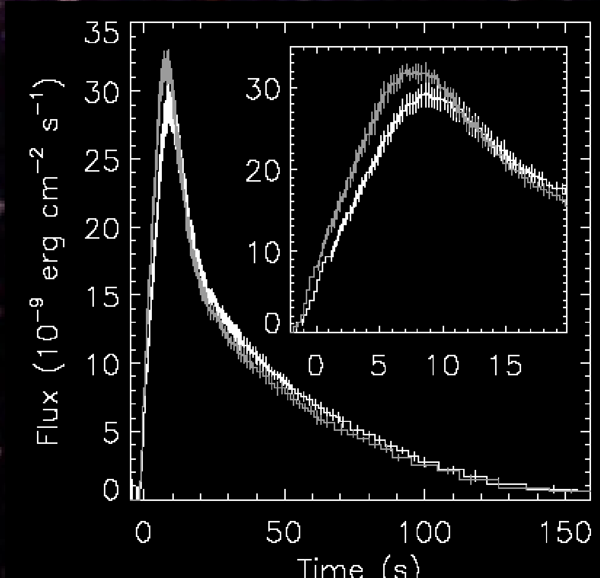

D.K. Galloway et al., ApJ 601 466 (2004).

Nucleosynthesis in XRBs

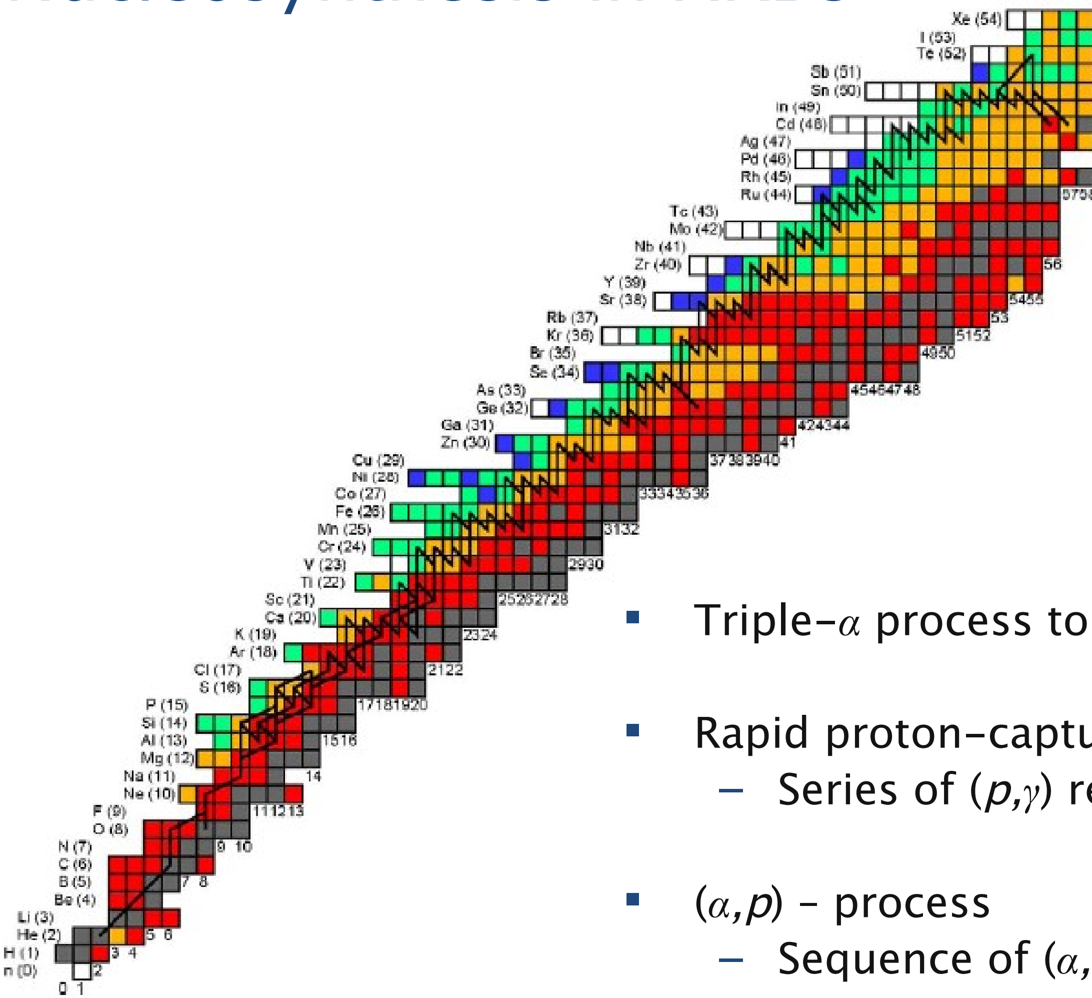

- Triple-α process to form ^{12}C
- Rapid proton-capture process (*rp* – process)
  - Series of (p,γ) reactions and β^+ – decays
- (α,p) – process
  - Sequence of (α,p) and (p,γ) reactions
- Reach nuclei far from stability, close to the proton-drip line

Waiting points in XRBs

- Potential waiting points in XRBs
  (Fisker, Schatz, Thielemann, ApJ SS 2008):
  - ^{22}Mg
  - ^{26}**Si**
  - ^{30}**S**
  - ^{34}**Ar**

- At lower temperatures, nuclei with low **(p,γ)** Q values come into **(p,γ)** – **(γ,p)** equilibrium

- If the **(α,p)** reaction rate is weak OR if the temperature is too low to overcome the Coulomb barrier for the **(α, p)** process, nuclear flow must await **β^+– decay** ($T_{1/2}$ = few seconds) before continuing on

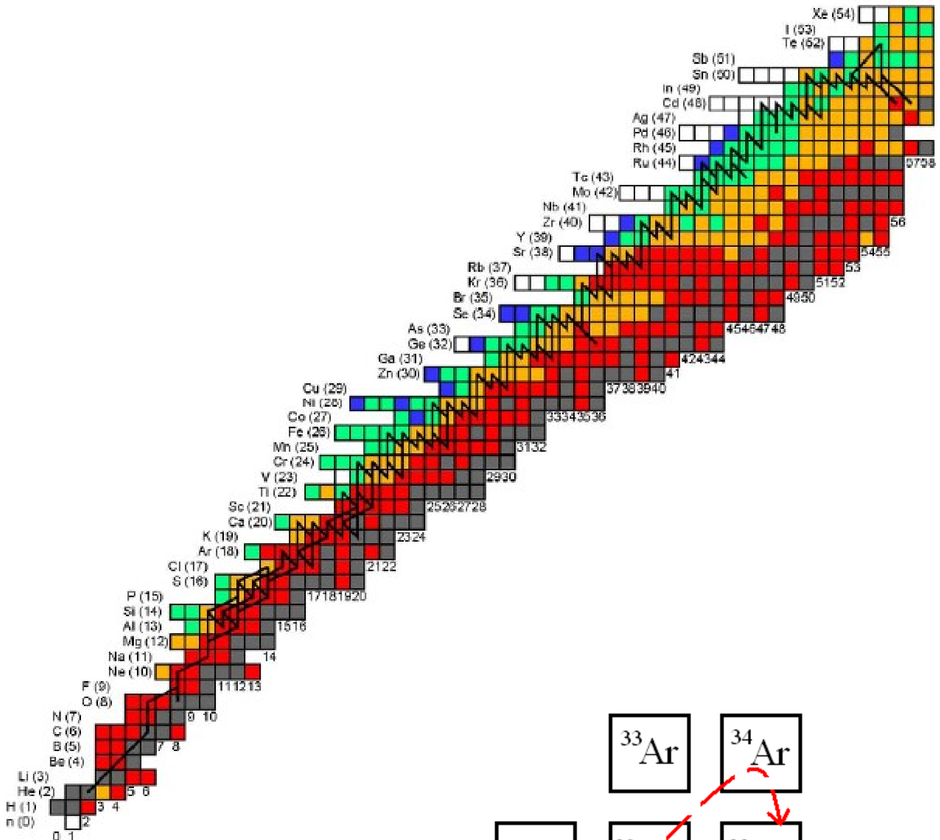

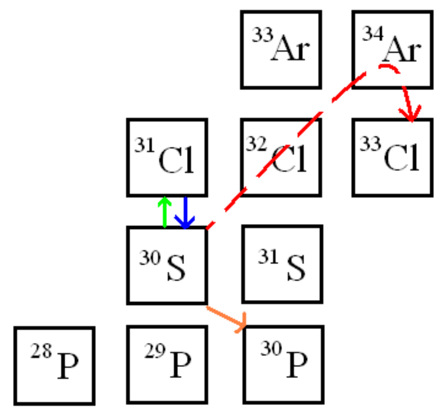

Waiting Point Effects

- Waiting points can affect the nucleosynthetic path
  - Final elemental abundances
  - Energy output during burst
  - Composition of neutron star surface → affects observables

- Luminosity profile can be affected due to pause in energy output as process pauses at waiting point
  - Leads to observed double-peak luminosity profiles

Table 19. Summary of the most influential nuclear processes, as collected from Tables 1–10. These reactions affect the yields of, at least, 3 isotopes when their nominal rates ar varied by a factor of 10 up and/or down. See text for details.

Reaction	Models affected
$^{12}C(\alpha,\gamma)^{16}O^{a}$	F08, K04-B2, K04-B4, K04-B5
$^{18}Ne(\alpha,p)^{21}Na^{a}$	K04-B1^{b}
$^{25}Si(\alpha,p)^{28}P$	K04-B5
$^{26g}Al(\alpha,p)^{29}Si$	F08
$^{29}S(\alpha,p)^{32}Cl$	K04-B5
$^{30}P(\alpha,p)^{33}S$	K04-B4
$^{30}S(\alpha,p)^{33}Cl$	K04-B4^{b}, K04-B5^{b}
$^{31}Cl(p,\gamma)^{32}Ar$	K04-B1
$^{32}S(\alpha,\gamma)^{36}Ar$	K04-B2
$^{56}Ni(\alpha,p)^{59}Cu$	S01^{b}, K04-B5
$^{57}Cu(p,\gamma)^{58}Zn$	F08
$^{59}Cu(p,\gamma)^{60}Zn$	S01^{b}, K04-B5
$^{61}Ga(p,\gamma)^{62}Ge$	F08, K04-B1, K04-B2, K04-B5, K04-B6
$^{65}As(p,\gamma)^{66}Se$	K04^{b}, K04-B1, K04-B2^{b}, K04-B3^{b}, K04-B4, K04-B5, K04-B6
$^{69}Br(p,\gamma)^{70}Kr$	K04-B7
$^{75}Rb(p,\gamma)^{76}Sr$	K04-B2
$^{82}Zr(p,\gamma)^{83}Nb$	K04-B6
$^{84}Zr(p,\gamma)^{85}Nb$	K04-B2
$^{84}Nb(p,\gamma)^{85}Mo$	K04-B6
$^{85}Mo(p,\gamma)^{86}Tc$	F08
$^{86}Mo(p,\gamma)^{87}Tc$	F08, K04-B6
$^{87}Mo(p,\gamma)^{88}Tc$	K04-B6
$^{92}Ru(p,\gamma)^{93}Rh$	K04-B2, K04-B6
$^{93}Rh(p,\gamma)^{94}Pd$	K04-B2
$^{96}Ag(p,\gamma)^{97}Cd$	K04, K04-B2, K04-B3, K04-B7
$^{102}In(p,\gamma)^{103}Sn$	K04, K04-B3
$^{103}In(p,\gamma)^{104}Sn$	K04-B3, K04-B7
$^{105}Sn(\alpha,p)^{108}Sb$	S01^{b}

Table 20. Nuclear processes affecting the total energy output by more than 5%, as well as the yield of at least one isotope, when their nominal rates are individually varied by a factor of 10 up and/or down, for the given model. See text for details.

Reaction	Models affected
$^{15}O(\alpha,\gamma)^{19}Ne^{a}$	K04, K04-B1, K04-B6
$^{18}Ne(\alpha,p)^{21}Na^{a}$	K04-B1, K04-B6
$^{22}Mg(\alpha,p)^{25}Al$	F08
$^{23}Al(p,\gamma)^{24}Si$	K04-B1
$^{24}Mg(\alpha,p)^{27}Al^{a}$	K04-B2
$^{26g}Al(p,\gamma)^{27}Si^{a}$	F08
$^{28}Si(\alpha,p)^{31}P^{a}$	K04-B4
$^{30}S(\alpha,p)^{33}Cl$	K04-B4, K04-B5
$^{31}Cl(p,\gamma)^{32}Ar$	K04-B3
$^{32}S(\alpha,p)^{35}Cl$	K04-B2
$^{35}Cl(p,\gamma)^{36}Ar^{a}$	K04-B2
$^{56}Ni(\alpha,p)^{59}Cu$	S01
$^{59}Cu(p,\gamma)^{60}Zn$	S01
$^{65}As(p,\gamma)^{66}Se$	K04, K04-B2, K04-B3
$^{69}Br(p,\gamma)^{70}Kr$	S01
$^{71}Br(p,\gamma)^{72}Kr$	K04-B7
$^{103}Sn(\alpha,p)^{106}Sb$	S01

[a]Reaction experimentally constrained to better than a factor of ~10 at XRB temperatures. See Section 5.

A. Parikh *et al.*, ApJ SS (2008).

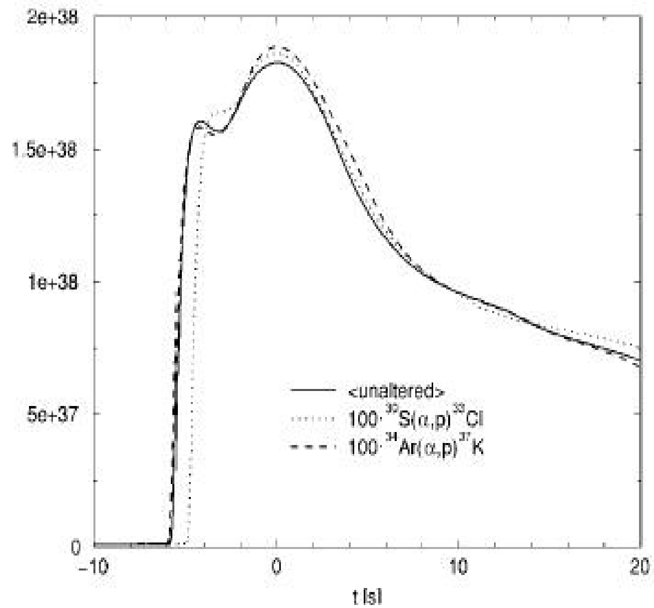

J.L. Fisker, F.K. Thielemann, and M. Wiescher ApJ 608, L61 (2004).

Reaction Rates in XRBs

- Current models and studies are based on theoretical Hauser-Feschbach reaction rates → **Almost no experimentally obtained information is known**
  - NIC_XI_366, NIC_XI_098
  - O'Brien *et al.*, AIP Conf. Proc. 2009

- Given the current limitations of radioactive beam facilities most *rp*- and α, *p*-process reactions are inaccessible

- Radioactive beams close to stability can be produced at ATLAS via the "in-flight" technique

- Studied (α,p) reactions on potential waiting points using time-inverse and inverse kinematic reactions:
  - $p(^{29}\mathrm{P},{}^{26}\mathrm{Si})\alpha$
  - $p(^{33}\mathrm{Cl},{}^{30}\mathrm{S})\alpha$
  - $p(^{37}\mathrm{K},{}^{34}\mathrm{Ar})\alpha$

Experimental Setup

- Beams produced by ATLAS
  - Stable beam produced in ECR source and accelerated
  - **Radioactive ion beam (RIB)** produced via "in-flight" technique

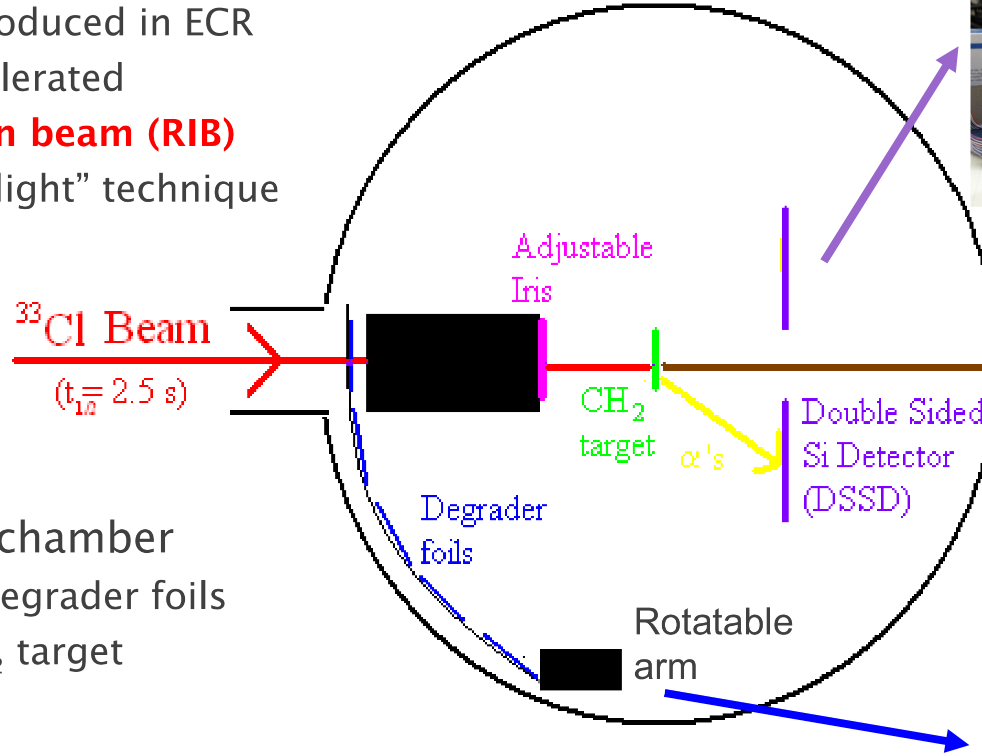

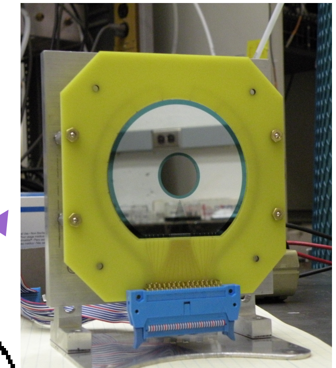

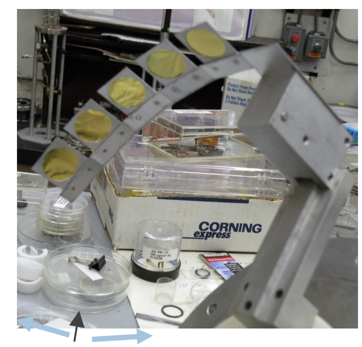

- RIB enters target chamber
  - Slowed by Au degrader foils
  - Incident on CH_2 target

- Reaction products detected in coincidence
  - α-particles detected in Double-Sided Si Detector (DSSD)
  - Heavier reaction products separated by Enge SplitPole Spectrograph used in gas-filled mode and detected in Parallel Grid Avalanche Counter (PGAC) and ionization chamber at focal plane of spectrograph

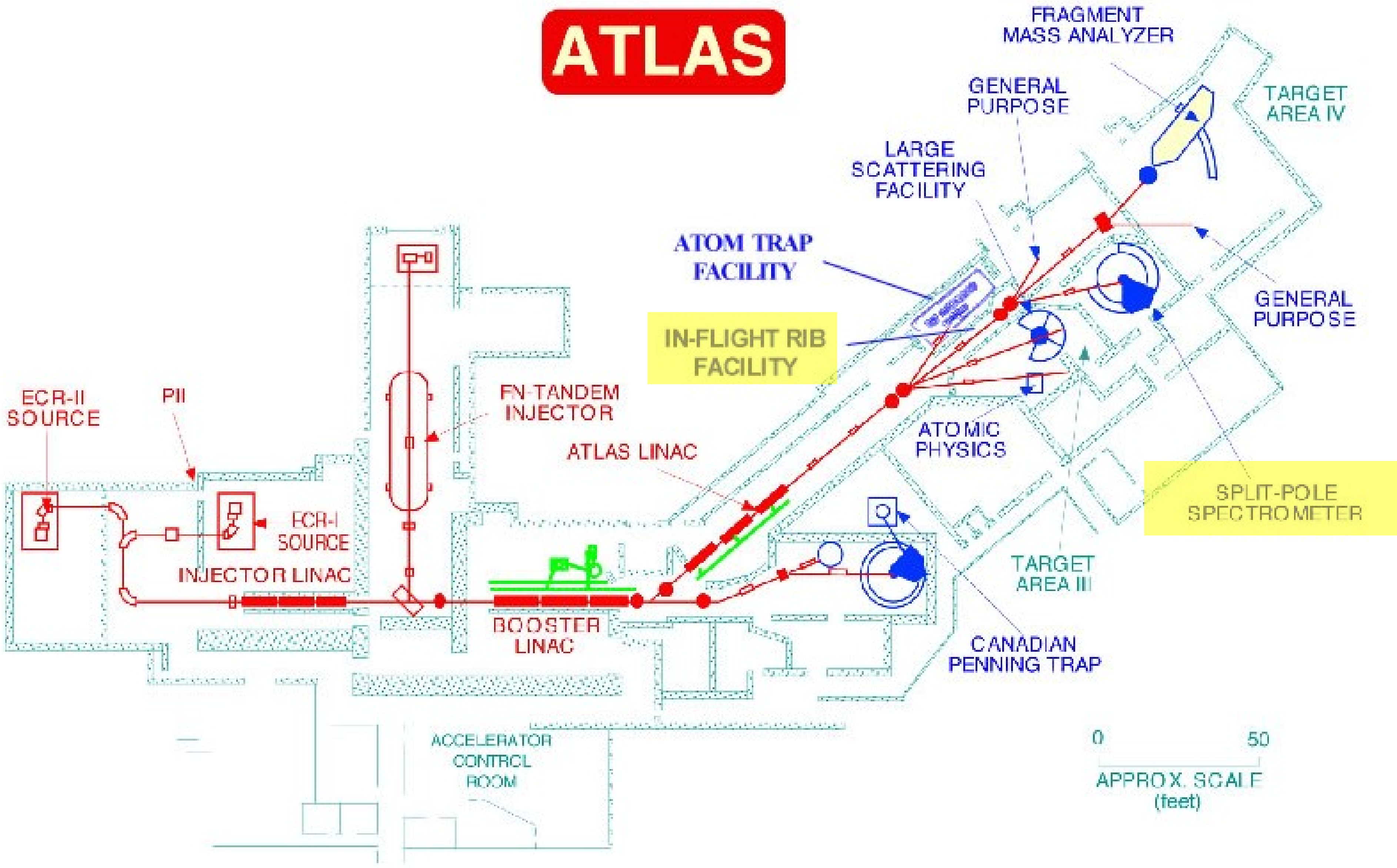
ATLAS
FRAGMENT MASS ANALYZER
GENERAL PURPOSE
TARGET AREA IV
LARGE SCATTERING FACILITY
ATOM TRAP FACILITY
GENERAL PURPOSE
IN-FLIGHT RIB FACILITY
ECR-II SOURCE
PII
FN-TANDEM INJECTOR
ATLAS LINAC
ATOMIC PHYSICS
SPLIT-POLE SPECTROMETER
ECR-I SOURCE
INJECTOR LINAC
TARGET AREA III
BOOSTER LINAC
CANADIAN PENNING TRAP
ACCELERATOR CONTROL ROOM
0
50
APPROX. SCALE (feet)

"In-Flight" Technique

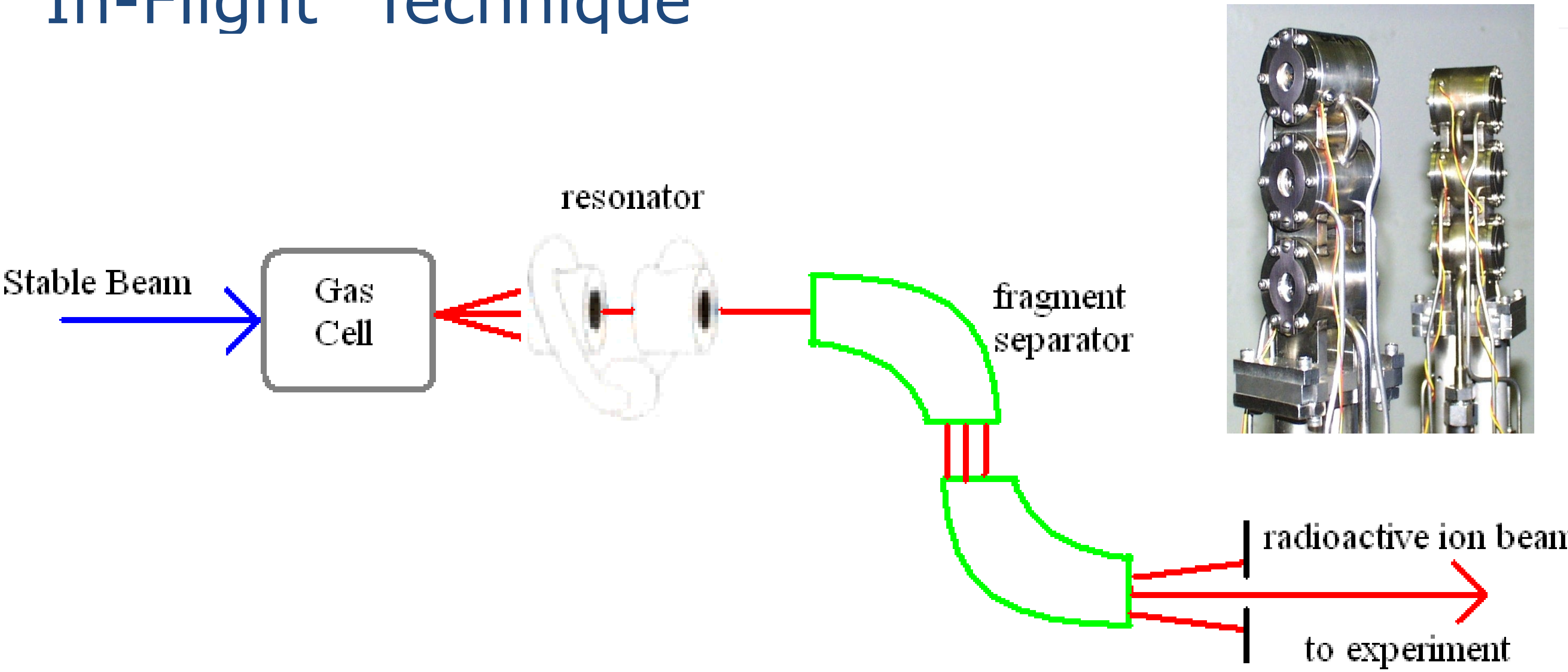

- Examples: ^{6}He, ^{7}Be, ^{8}Be, ^{8}Li, ^{11}C, ^{14}O, ^{16}N, ^{17}F, ^{20,21}Na, ^{25}Al, **^{29}P**, **^{33}Cl**, and **^{37}K**
- $^{32}S^{13+}$ stable primary beam
- Gas cell filled with deuterium
- ^{32}S(d,n)^{33}Cl produces $^{33}Cl^{17+}$ radioactive beam

^{33}Cl beam production

- Resulting beam is a cocktail of $^{32}S^{13+}$, $^{32}S^{14+}$, $^{32}S^{15+}$, $^{32}S^{16+}$, and $^{33}Cl^{17+}$
- $^{33}Cl^{17+}$ Tuned with ΔE – E telescope
  - Si Surface Barrier (SSB) detectors
    - ΔE 20 μm thick
    - E 150 μm thick
- RF sweeper is used to eliminate much of the contaminant ^{32}S beam
- Final ^{33}Cl beam intensity of 1.67×10^4 pps

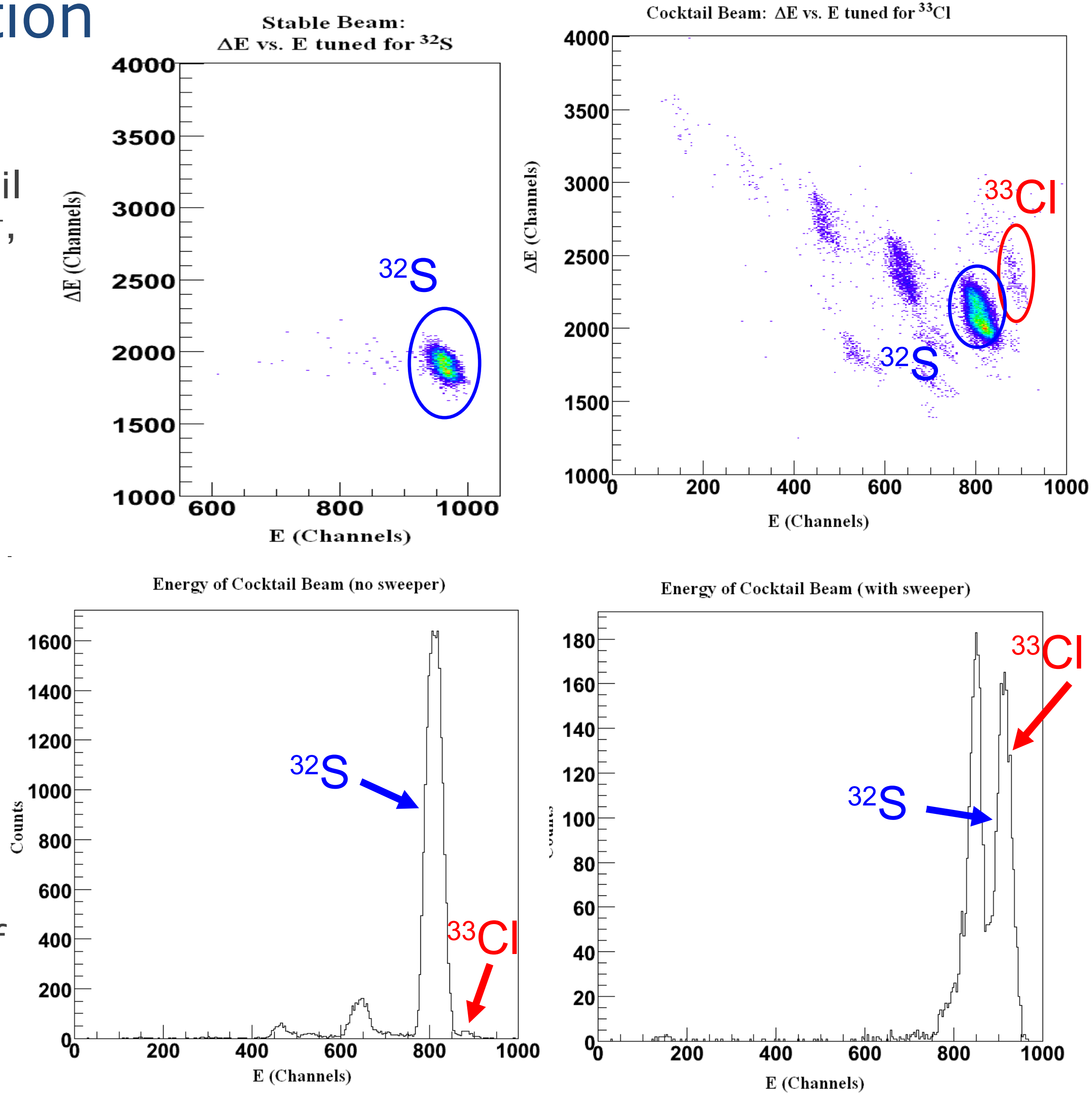

Experimental Setup

- Beams produced by ATLAS
  - Stable beam produced in ECR source and accelerated
  - Radioactive ion beam (RIB) produced via “in-flight” technique

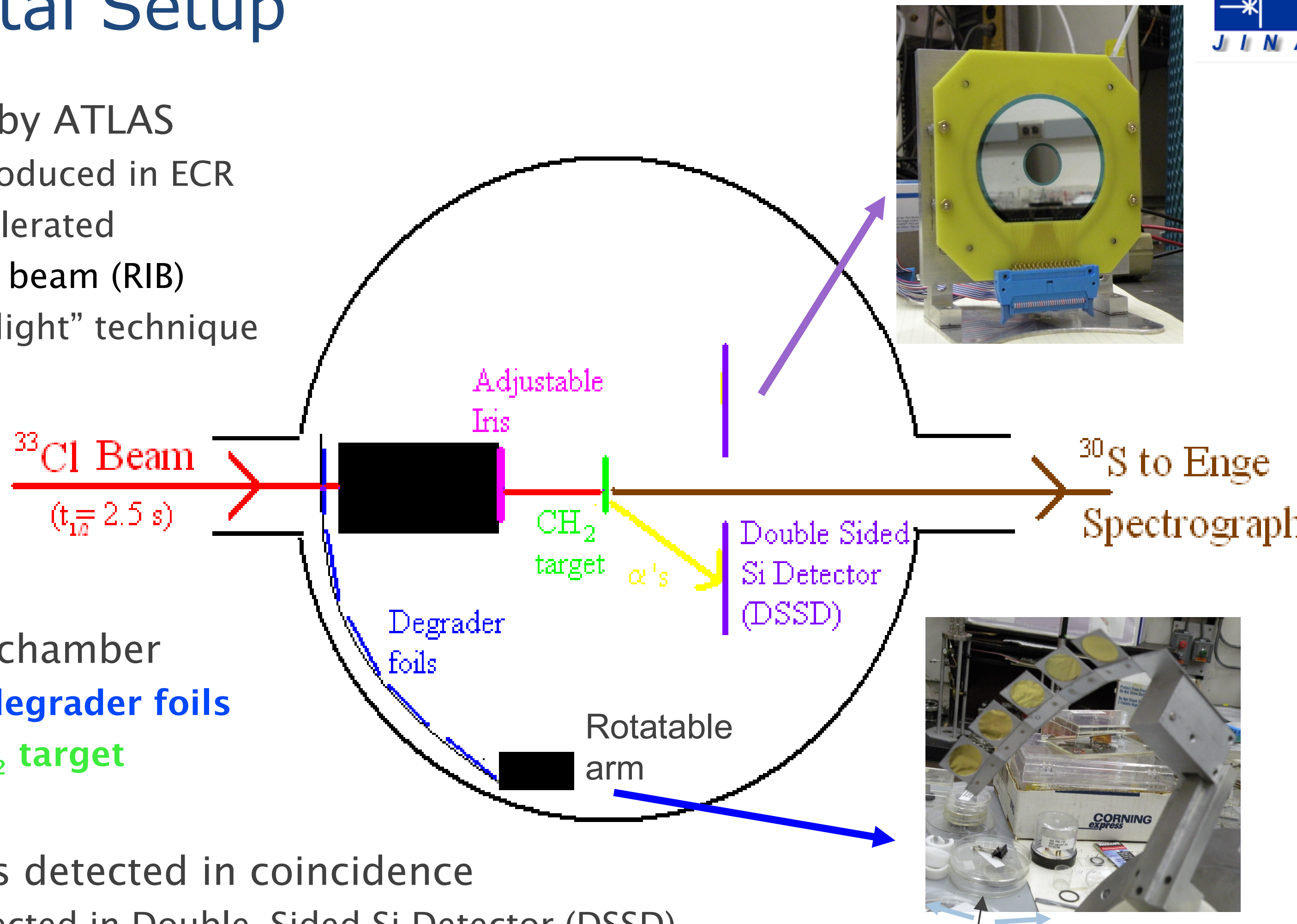

- RIB enters target chamber
  - Slowed by **Au degrader foils**
  - Incident on **CH_2 target**

- Reaction products detected in coincidence
  - α-particles detected in Double-Sided Si Detector (DSSD)
  - Heavier reaction products separated by Enge SplitPole Spectrograph used in gas-filled mode and detected in Parallel Grid Avalanche Counter (PGAC) and ionization chamber at focal plane of spectrograph

Experimental Setup

- Beams produced by ATLAS
  - Stable beam produced in ECR source and accelerated
  - Radioactive ion beam (RIB) produced via "in-flight" technique

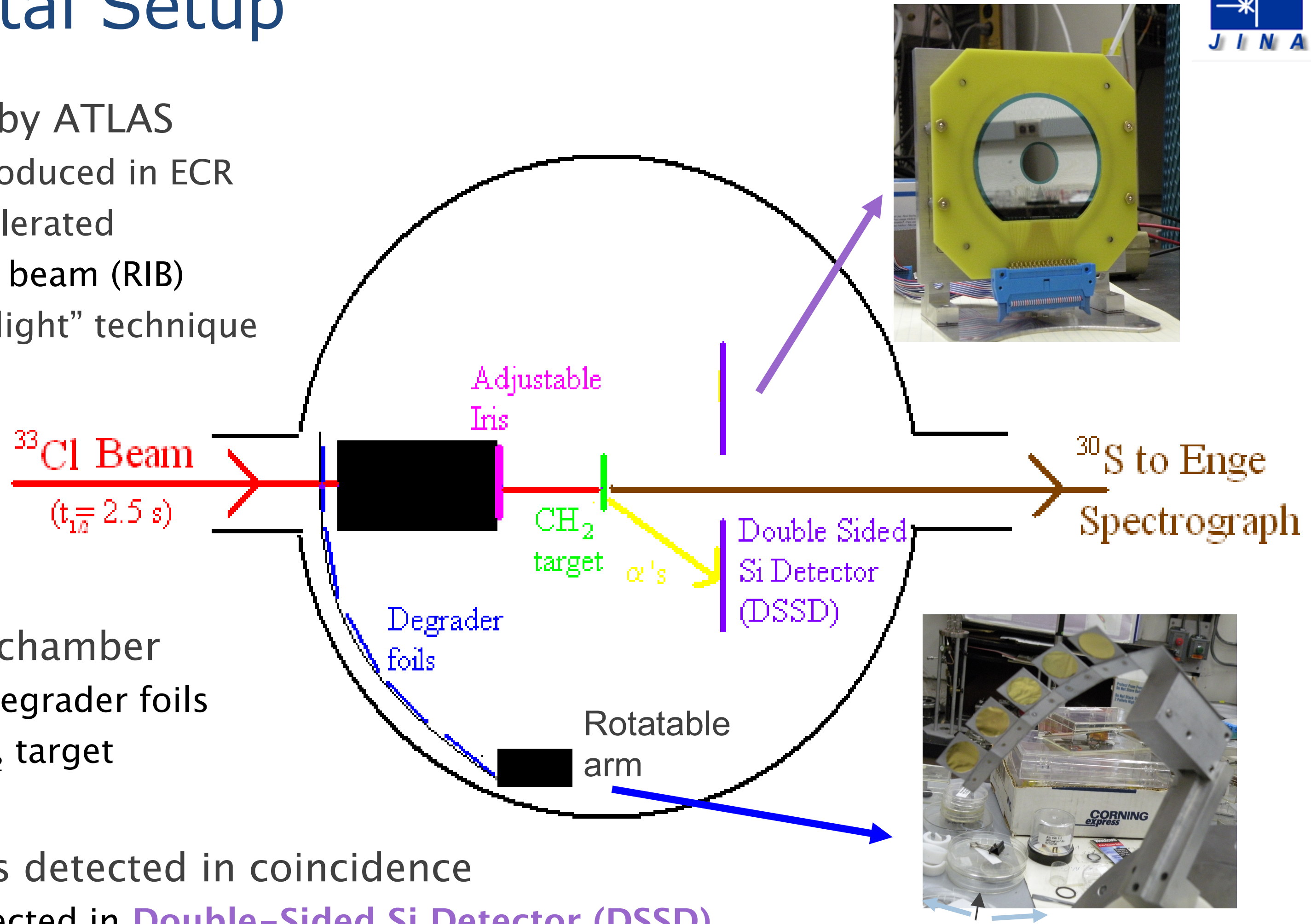

- RIB enters target chamber
  - Slowed by Au degrader foils
  - Incident on CH_2 target
- Reaction products detected in coincidence
  - α-particles detected in **Double-Sided Si Detector (DSSD)**
  - Heavier reaction products separated by Enge SplitPole Spectrograph used in gas-filled mode and detected in Parallel Grid Avalanche Counter (PGAC) and ionization chamber at focal plane of spectrograph

Experimental Setup

- Beams produced by ATLAS
  - Stable beam produced in ECR source and accelerated
  - Radioactive ion beam (RIB) produced via “in-flight” technique

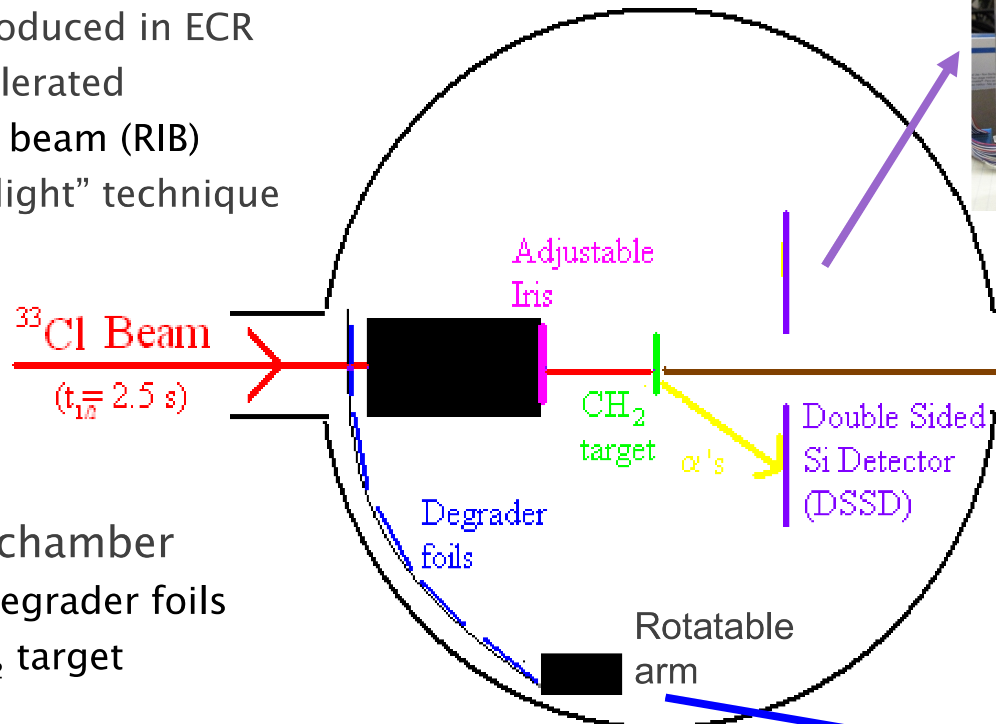

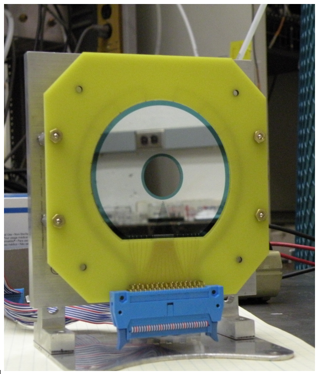

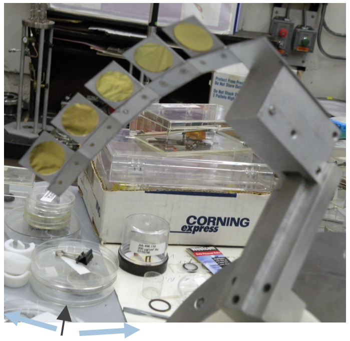

- RIB enters target chamber
  - Slowed by Au degrader foils
  - Incident on CH_2 target

- Reaction products detected in coincidence
  - α-particles detected in Double-Sided Si Detector (DSSD)
  - **Heavier reaction products separated by Enge SplitPole Spectrograph used in gas-filled mode and detected in Parallel Grid Avalanche Counter (PGAC) and ionization chamber at focal plane of spectrograph**

Proof of Principle with stable beam reactions: $p(^{33}S,^{30}P)\alpha$

- Using the same setup the $p(^{33}S,^{30}P)\alpha$ reaction was studied with a stable ^{33}S beam
- Gating on the ^{30}P–α coincidences and particle groups gives clear kinematic curves
- Data shown for multiple energy points
- Blue curves represent kinematic simulations

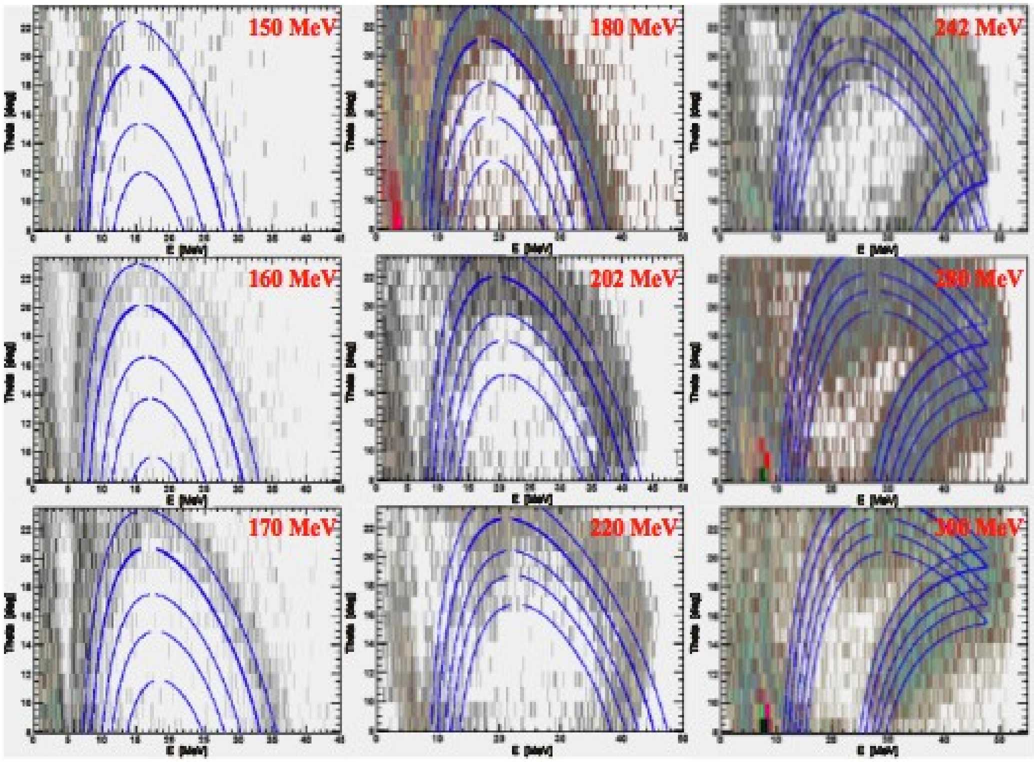

$p(^{33}Cl,^{30}S)\alpha$ Data

- $^{30}S - \alpha$ coincidences seen as well defined timing peak
- Using radioactive ^{33}Cl beam, particle ID is more difficult due to diffuseness of beam

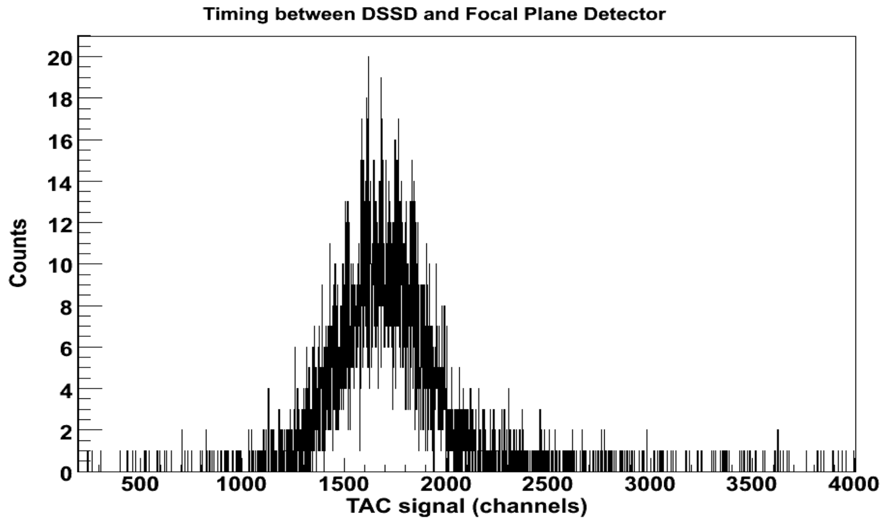

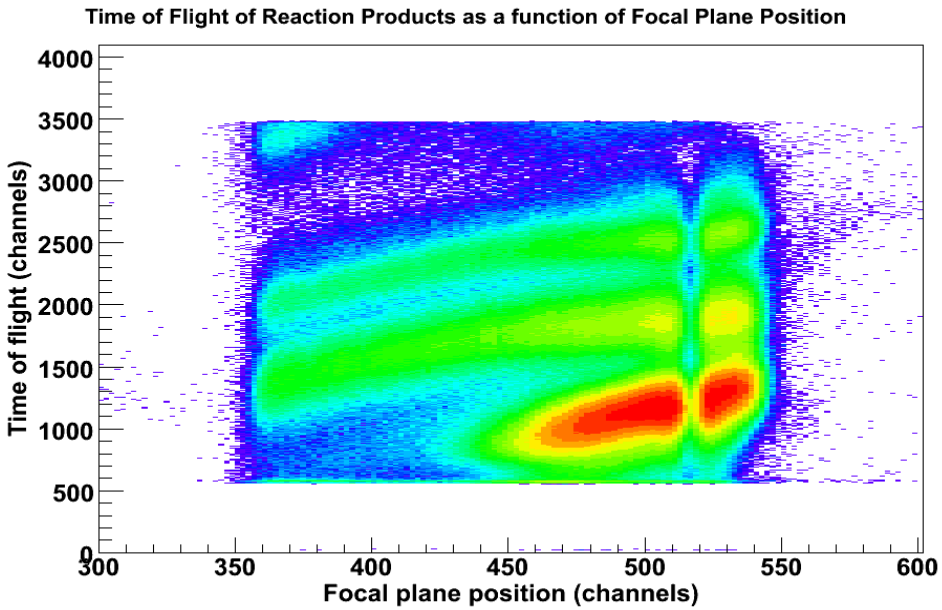

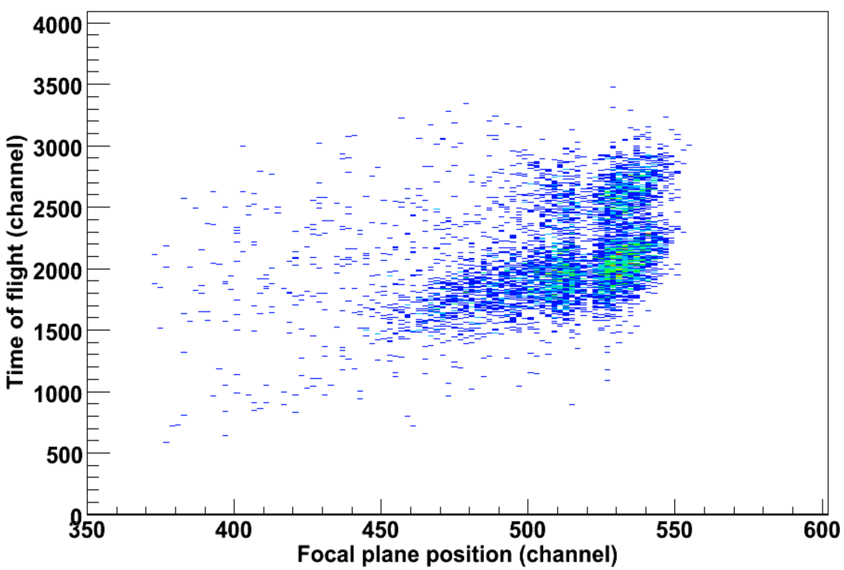

$p(^{33}Cl,^{30}S)\alpha$ Results: Simulations vs. Experiment

Monte Carlo Kinematic Simulation

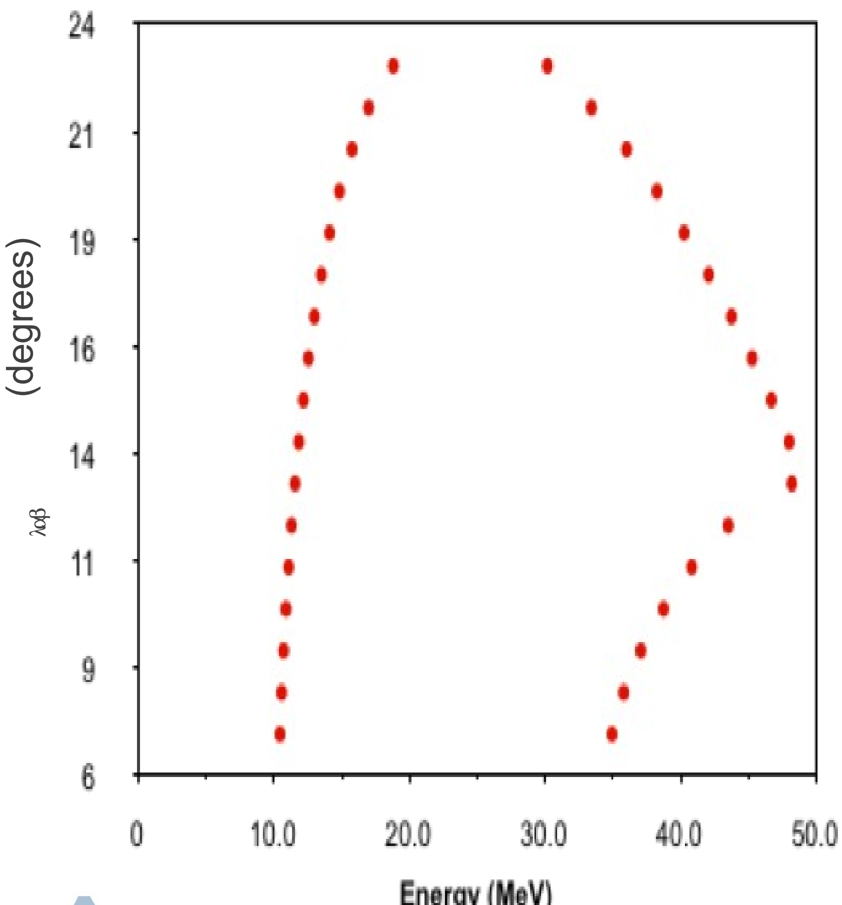

Experimental Data

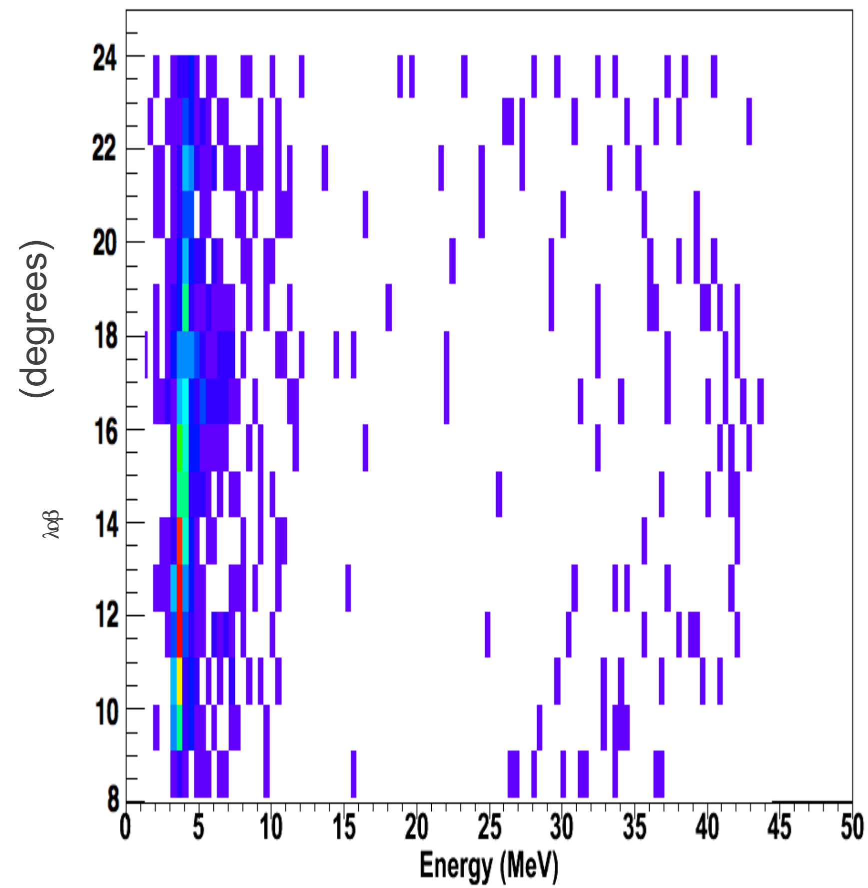

$p(^{33}Cl,^{30}S)\alpha$ Results

- Normalized via
  - Rutherford scattering
  - Direct beam measurements in spectrograph
  - Two methods agree within 10%

- Measurements made at three different energy points

- NON-SMOKER code give cross sections based on Hauser-Feshbach models (similar to those used in models where experimental information is not available)

- Measurements at lower energies are needed for x-ray burst models

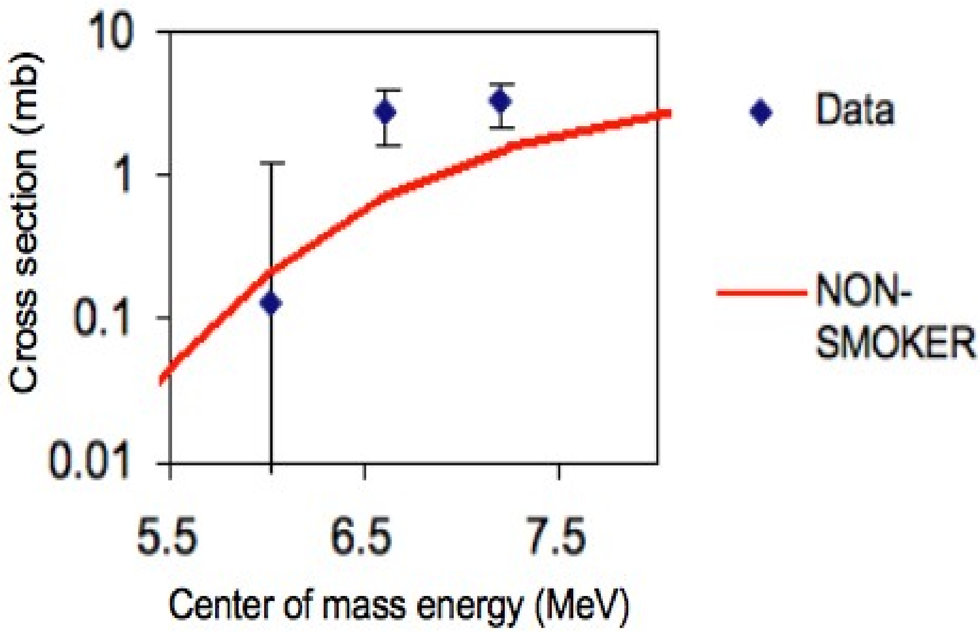

$p(^{37}K,^{34}Ar)\alpha$ Results (PRELIMINARY)

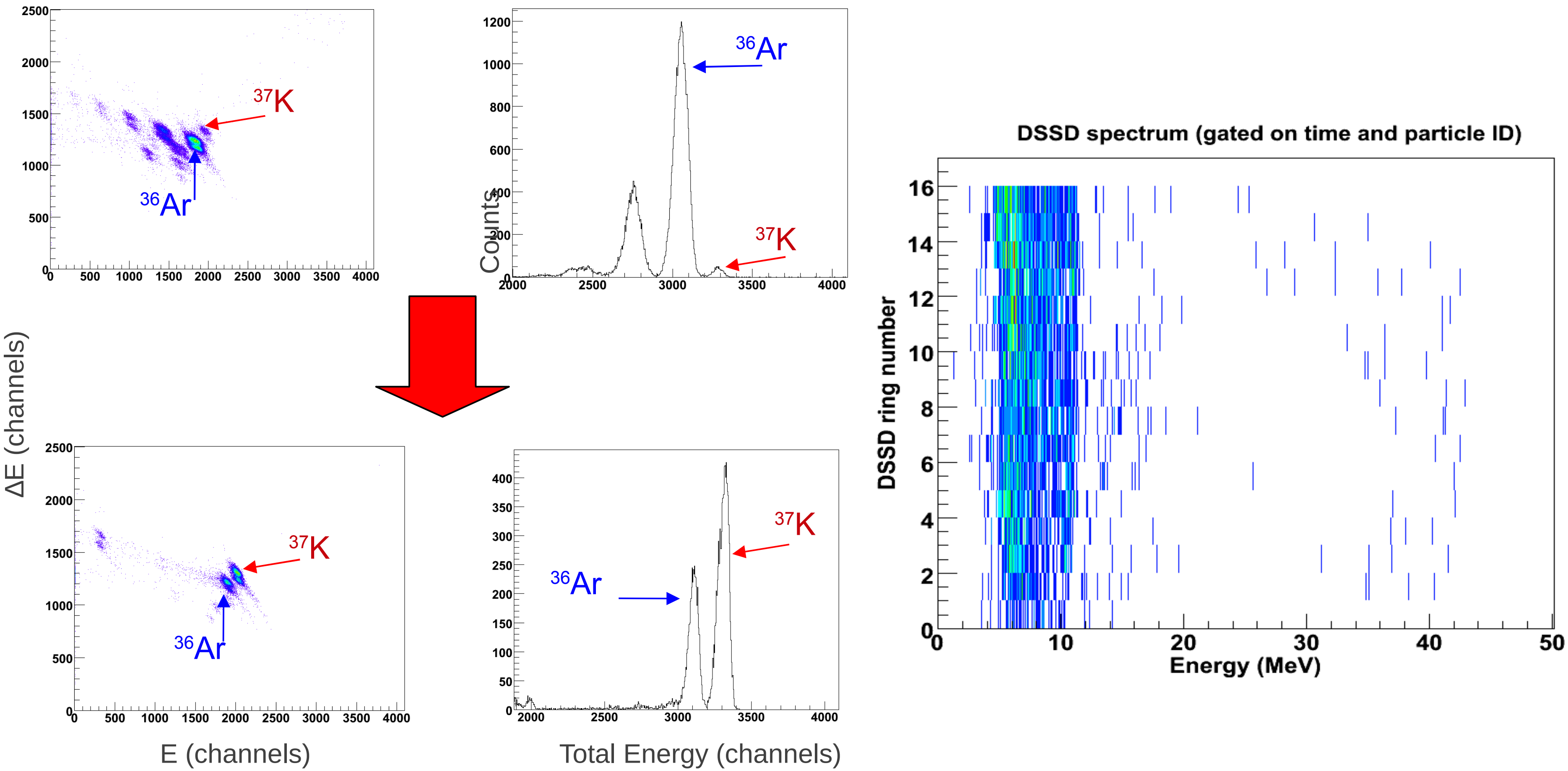

^{29}P beam development and preliminary $p(^{29}\mathrm{P},^{26}\mathrm{Si})\alpha$ run (June 2010)

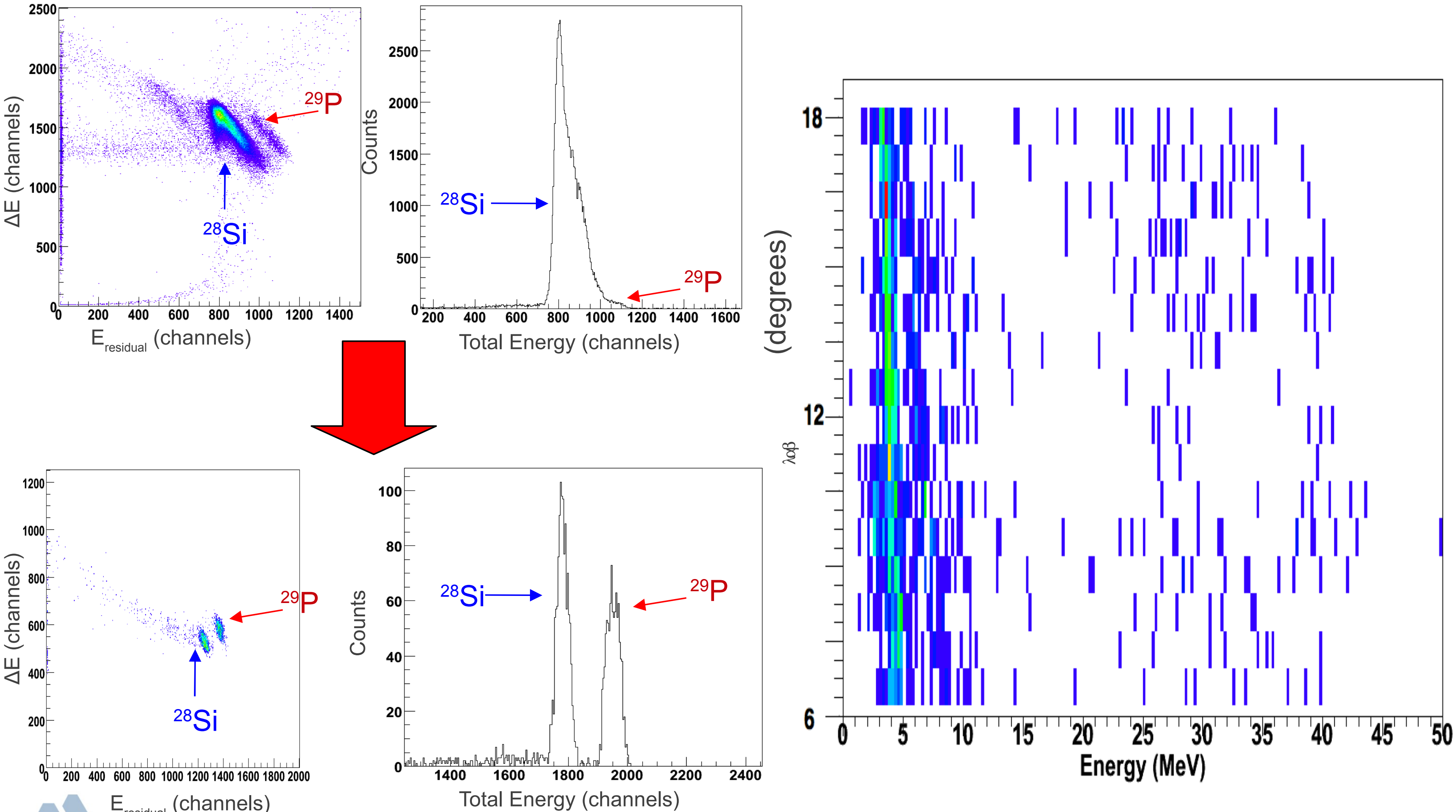

Summary and Future Plans

- $^{30}S(\alpha,p)^{33}Cl$ reaction rate affects
  - nucleosynthesis in XRBs
  - the energy output of XRBs
  - the luminosity of double-peaked XRBs

- $^{34}Ar(\alpha,p)^{37}K$ and $^{26}Si(\alpha,p)^{29}P$ is also a possible waiting point that may affect the double-peaked structure of luminosity profiles

- Radioactive ^{29}P, ^{33}Cl and ^{37}K beams have been produced at ATLAS

- Inverse kinematic studies of (α,p) reactions has been successfully completed using the Enge SplitPole Spectrograph and cross sections for three energy points have been measured for the $^{30}S(\alpha,p)^{33}Cl$ and $^{34}Ar(\alpha,p)^{37}K$ reactions; One energy point for the $^{26}Si(\alpha,p)^{29}P$ reaction, which is currently being studied

- More energy points, in the astrophysical range, should be measured in the future

- Measurements of other waiting point nuclei ^{22}Mg

- Direct (α,p) measurements using HELIOS with a gas target...?

Thank You!!

- ANL
  - Martin Alcorta
  - Peter Bertone
  - Jason Clark
  - John Greene
  - Calem Hoffman
  - Cheng-Lie Jiang
  - Ben Kay
  - Hye-Young Lee
  - Richard Pardo
  - Ernst Rehm
  - Claudio Ugalde
  - Gary Zinkann

- Colorado School of Mines/ANL
  - Nidhi Patel (graduate student)
- Western Michigan University
  - Shad Bedoor (graduate student)
  - John Lighthall (graduate student)
  - Scott Marley (graduate student)
  - Dinesh Shetty
  - Alan Wuosmaa
- TANDAR Laboratory, Argentina
  - Juan Manuel Figueira (graduate student)
- Hebrew University, Israel
  - Michael Paul

ATLAS staff and operators